Available online at www.sciencedirect.com
SCIENCE DIRECT®
Composite Structures 70 (2005) 185–199
COMPOSITE STRUCTURES
www.elsevier.com/locate/compstruct

FRPC reinforced concrete beam-column joints under cyclic excitation

Abhijit Mukherjee *, Mangesh Joshi

Department of Civil Engineering, Indian Institute of Technology Bombay, Mumbai 400 076, India

Available online 29 September 2004

Abstract

An investigation on the performance of reinforced concrete beam-column joints under cyclic loading is reported. Joints have been cast with adequate and deficient bond of reinforcements at the beam-column joint. FRP sheets and strips have been applied on the joints in different configurations. The columns are subjected to an axial force while the beams are subjected to a cyclic load with controlled displacement. The amplitude of displacement is increased monotonically using a dynamic actuator. The hysteretic curves of the specimens have been plotted. The energy dissipation capacity of various FRP configurations has been compared. In addition, the control specimens have been reused after testing as damaged specimens that are candidates for rehabilitation. The rehabilitation has been carried out using FRP and their performance has been compared with that of the undamaged specimens.

Keywords: Structural upgradation; Fiber reinforced polymer composites; Concrete; Beam-column joints; Cyclic loading; Hysteretic curves; Energy absorption

1. Introduction

Although hundreds of thousands of successful reinforced cement concrete (RCC) framed structures are annually constructed worldwide, there are large numbers of them that deteriorate, or become unsafe due to changes in loading, changes in use, or changes in configuration. Occurrence of natural calamities may also lead to review of engineering notions that make reworking of existing structures inevitable. The reworking is variously referred as repair, rehabilitation, retrofitting, and upgradation with distinct meanings attached to all these terminologies. In this paper, we use *upgradation* to suggest all these activities. The RCC beam-column joints may require upgradation due to deficient detailing of reinforcing bars, insufficient column sections or due to increased loading on the structure. Upgradation of these joints, however, is a challenging task that poses major practical difficulties. A variety of techniques have been applied to joints with the most common ones being the construction of RCC or steel jackets [1,2]. Reinforced concrete jackets require intensive labor and often intricate detailing of steel in the form of diagonal collars. Moreover, concrete jackets increase the dimensions and weight of structural elements. Few attempts have been made in employing plain or corrugated steel plates [3,4]. In addition to corrosion protection, these elements require special attachment through the use of either epoxy adhesives combined with bolts or special grouting.

FRPC based strengthening strategy could be an attractive option in order to restore the joints. In addition to being lighter, thinner and easier to implement FRPC reinforced joints have the virtue of making the joints more ductile. This property is extremely desirable for seismic upgradation of structures. However, a direct extension of the strategies adopted for beams and columns is difficult as the behavior of beam-column connections is complex and still not completely understood.

* Corresponding author. Tel.: +91 22 2576 7343/578 2545; fax: +91 22 576 7302/578 3480.
E-mail address: abhijit@civil.iitb.ac.in (A. Mukherjee).

0263-8223/$ - see front matter © 2004 Elsevier Ltd. All rights reserved.
doi:10.1016/j.compstruct.2004.08.022

Research on this area can be classified into experiments with quasistatic loading on bridge beam-column joints [5,6], typical building frame joints [7,8] and frameworks [9] report enhancement of both shear and bending capacity. Cyclic load tests on joints with inadequate reinforcement bond length [10], rehabilitated specimens [11], shear strengthened T joints [12–14], have also reported substantial improvements in ultimate capacities. A combination of FRP in various forms bars, plates and sheets in structural enhancement have been investigated [15,16]. The suitability of adhesives of different moduli [17] has also been studied. On some occasions a combination of FRP and steel external reinforcements has been used [18]. FRP in seismic retrofitting of strong-beam-weak-column frameworks that are prevalent in gravity load designed buildings have been investigated [19].

Analytical models of externally reinforced beam-column joints have been presented using closed form solutions [20], and finite element technique [21]. Design methods have been suggested for shear [22] and bending [20]. Pushover analysis has been employed in the design of upgradation for bridge joints [21] and buildings [23] in seismic conditions.

Survey of existing constructions reveals that upgradation of structures is necessary in three conditions:

- The structure is inadequately designed for the present load conditions.
- The structure is inadequately detailed for the present loading. This also includes those structures that are found deficient under seismic conditions.
- The structure is damaged and requires rehabilitation.

This paper includes joints of all the three varieties. The motivation behind this program is to examine the performance of fiber reinforced polymer composites (FRP) in upgradation of healthy joints with adequate and deficient reinforcements and also in rehabilitation of damaged joints. The load deflection relations obtained experimentally are discussed along with failure types.

2. Experimental work

2.1. Specimen details

Two different types of RCC joints have been cast for experimental verification. One set of joints has adequate steel reinforcements with proper detailing of reinforcements at the critical sections (Fig. 1). In the other set of specimens the beam reinforcements have deficient bond lengths at the junctions with the columns (Fig. 2). When the beam of the joint is transversely loaded the first set is characterized by a long plastic zone (ductile) while the second set fails in reinforcement pull out and exhibits sudden failure (non-ductile).

The concrete used is of M30 grade (30 N/mm^2) and properties of other material used are shown in Table 1.

2.2. FRP reinforcements

The specimens in Figs. 1 and 2 were strengthened by using carbon and glass FRP materials. Prior to the application of the FRP the concrete substrate was smoothed by grinding and cleaning. The cement paste was removed from the surface and the coarse aggregates were exposed. Acetone was used to clean the surface. The corners of all the members were ground to create a minimum radius of 10 mm. Epoxy putty was used to fill the voids and concave areas. Figs. 3 and 4 present schematic arrangement for two typical systems; L-overlays and precured carbon plates respectively.

2.3. Type A: L-reinforcement with GFRP/CFRP sheets

In this type, FRP sheets were applied in L shape to upgrade the joints. FRP has been applied in several

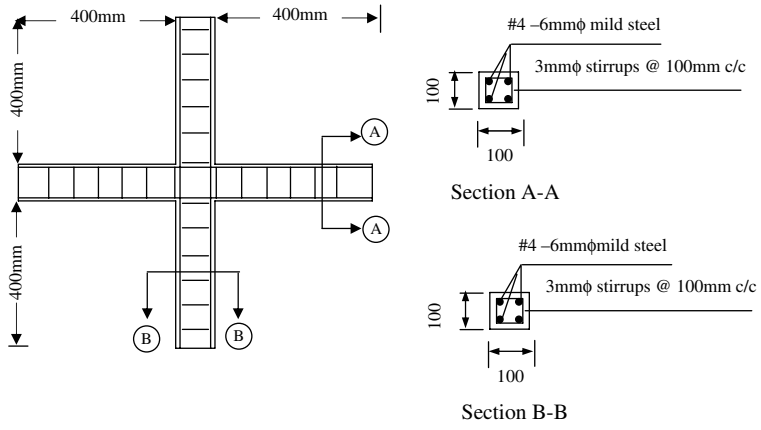

Fig. 1. Specimen with ductile joint reinforcement.

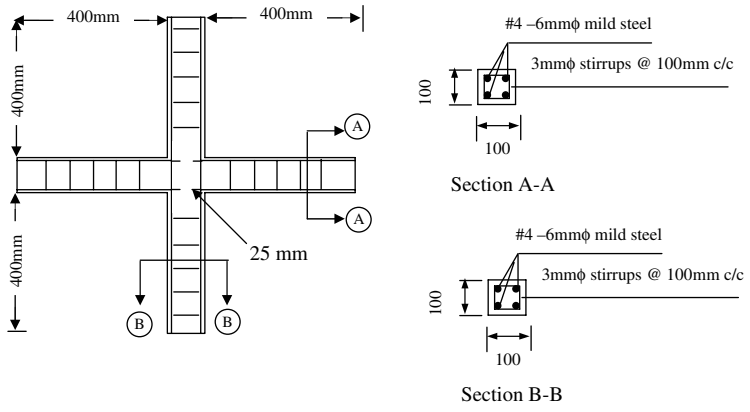

Fig. 2. Specimen with non-ductile joint reinforcement.

Table 1
Properties of materials

Material	Effective thickness (mm)	Ultimate strength (MPa)	Tensile modulus (GPa)	Ultimate strain
Glass—G (fiber)	0.36	2250	70	0.0239
Carbon—C (fiber)	0.11	3500	230	0.0117
Carbon plate—CP (composite)	1.2	2800	165	0.017
Mild steel longitudinal reinforcement	6 mm dia	275	198	0.045
Mild steel transverse reinforcement	3 mm dia	555.13	193	0.043

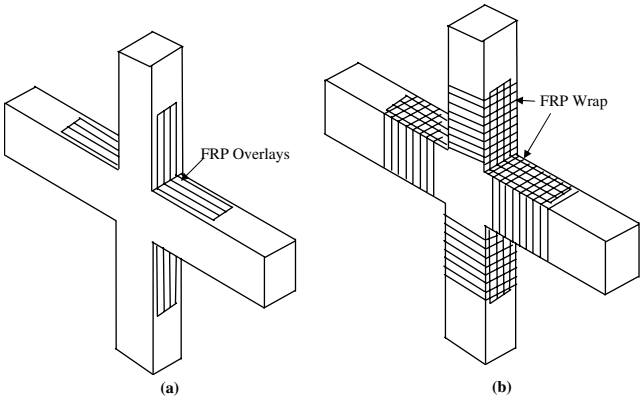

Fig. 3. Type A strengthening system—use of composite overlays.

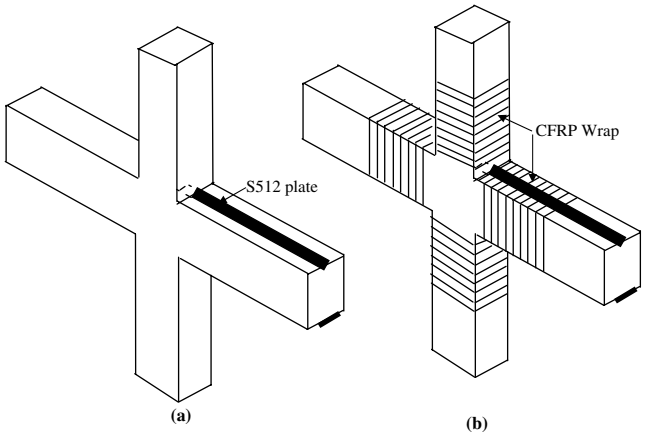

Fig. 4. Type B strengthening system—use of precured carbon plate.

layers. In step 1 FRP has been applied on the top and bottom surfaces concrete surfaces. The fibers were along the axes of the members (Fig. 3a). Subsequently, FRP wraps were provided over the inner layers (Fig. 3b). The direction of fibers in wraps was perpendicular to the axis of the members.

Each joint was used for two different lay ups. Fig. 5a shows glass fiber sheets (80 mm wide and 250 mm long) on either side of the joint. On one side only one layer is provided. On the other side two layers of FRP have been provided to evaluate the efficacy of different extents of upgradation. Both the column and the beam are then wrapped by unidirectional glass fibers with 100 mm lap length as shown in step 2 of Fig. 5. Same configuration is repeated using carbon fiber sheet using 1 and 2 layers of overlays and single wrap with 100 mm overlap. Both adequate and deficient joints were reinforced using this configuration.

2.4. Type B: reinforcement with plates

In this type, procured carbon plate (25 mm wide and 1.2 mm thick) have been used in the beams to improve bending stiffness. To achieve a good bond between the plate and the concrete beam at the joint a groove (25 mm wide and 25 mm deep) has been created inside the concrete joint. The plates have been inserted into the joint as shown in Fig. 6. The groove was left in the specimens at the time of casting. Surfaces of the concrete specimens were prepared as discussed earlier. The

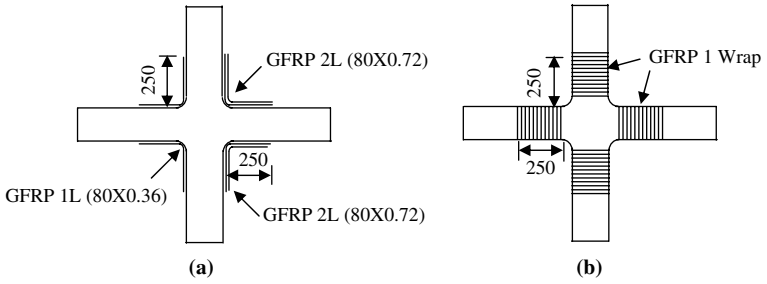

Fig. 5. Strengthening Type A with GFRP/CFRP Sheets.

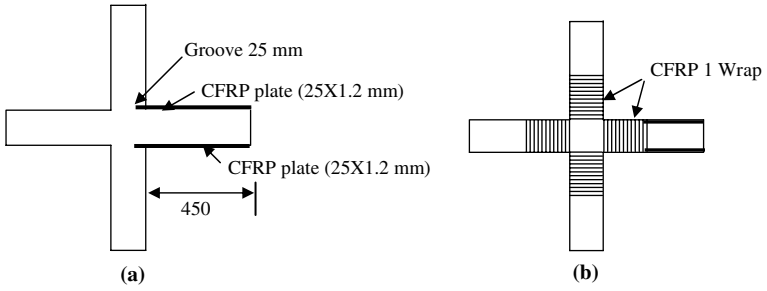

Fig. 6. Strengthening Type B.

groove was filled by injecting epoxy resin, and the plates were inserted in grove as shown in step 1 of Fig. 6. The beams and columns were then wrapped using a single wrap of carbon sheet.

2.5. Rehabilitated specimens

The control specimens without FRP were used after testing to evaluate the rehabilitation of joints with FRP. From the failed specimens loose concrete was removed and the cracks and voids were filled with epoxy and sand mortar. The smooth surfaces were restored prior to the application of FRP. Grooves were cut up to 25 mm depth using a rotary concrete cutter. Type B strengthening system with precured carbon plates was used.

The detailed test matrix for adequate and deficient specimens is presented in Tables 2 and 3 respectively.

Table 2
Test matrix for ductile specimen

S. no.	Specimen name	Details
1	D-1	–
2	G1L-D	Type A with single L of GFRP at top and bottom
3	G2L-D	Type A with two L of GFRP at top and bottom
4	C1L-D	Type A with single L of CFRP at top and bottom
5	C2L-D	Type A with two L of CFRP at top and bottom
6	CP1-D	Type B with CFRP plate at top and bottom
7	Rehab.	Type B with CFRP plate at top and bottom

Table 3
Test matrix for non-ductile specimen

S. no.	Specimen name	Details
1.	ND-1	–
2	G1L-ND	Type A with single L of GFRP at top and bottom
3	G2L-ND	Type A with two L of GFRP at top and bottom
4	C1L-ND	Type A with single L of CFRP at top and bottom
5	C2L-ND	Type A with two L of CFRP at top and bottom
6	CP1-D	Type B with CFRP plate at top and bottom

2.6. Test program

The experimental setup is as shown in Fig. 7. The column was fixed at its ends on a loading frame. It was subjected to a constant axial load of 100 KN which is 50% of ultimate load carrying capacity of the column. This is considered the service load that the column is expected to carry under normal loading conditions.

Cyclic load was applied using a hydraulic actuator. The load cycle was predefined as shown in Fig. 8. The displacement started from the neutral position and it oscillated harmonically about that position. It increased at a uniform rate 0.25 mm/cycle. Each cycle comprises of three full waves of same amplitude in 10 s (0.3 Hz. frequency). The final tip deflection was 22.5 mm. The other end of the beam was free. Vertical deflection of the tip of the beam was recorded directly by the linear variable displacement transducer (LVDT) built in the actuator. It was validated with another external LVDT. The data were collected using a computerized data acquisition system.

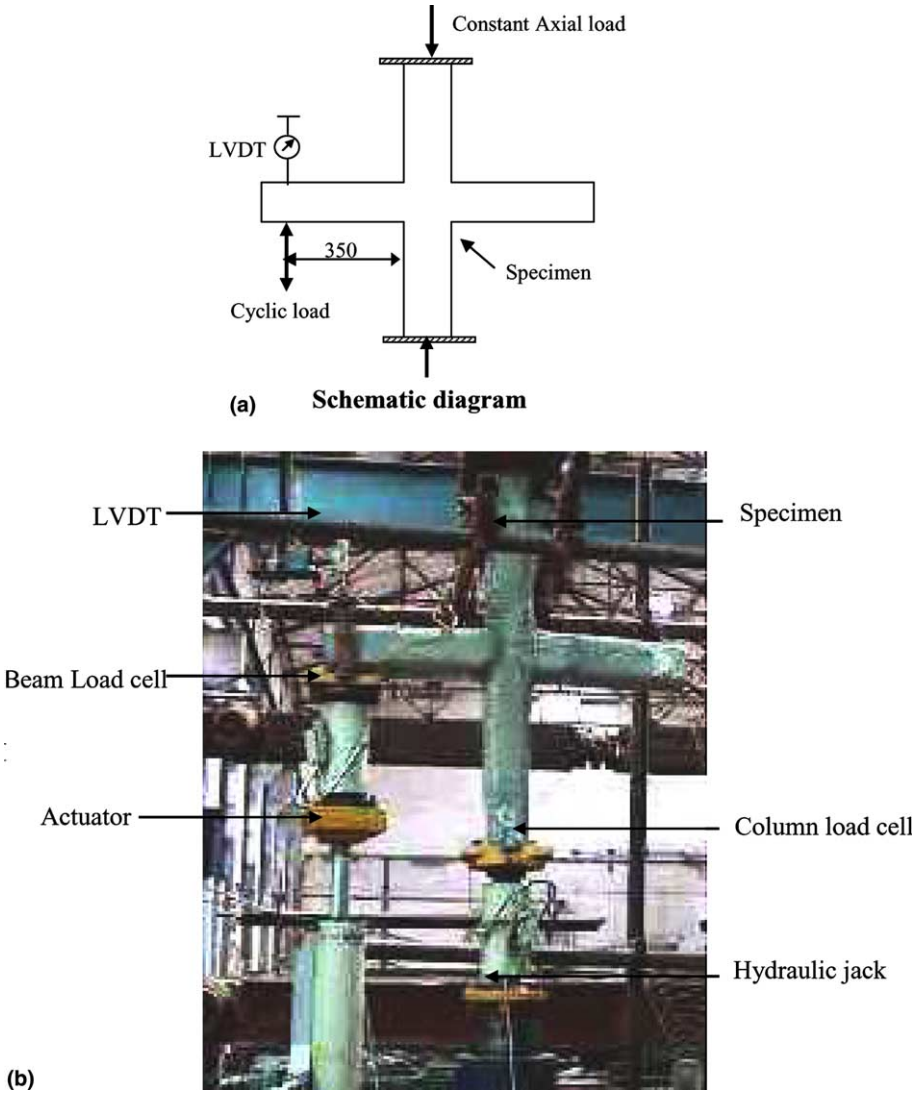

Fig. 7. Experimental setup.

3. Results and discussion

The beam tip load–displacement characteristics for all the specimens are discussed here. The displacement levels of the first few cycles did not generate any nonlinear deformation in the structure and the loops followed a straight line with its slope as initial stiffness. The onset of stiffness degradation was identified by simultaneous appearance of tension cracks at the root of the cantilever beam. The calculations show that at this point the steel started to yield and it was not capable of taking any further load. The additional load from this point was carried by the FRP. At this point linearity of the ascending and the descending paths was lost and loops between the two paths appeared. We term this phenomenon *yield*. The post yield behavior is signified by monotonic degradation of stiffness. To enable comparison among different systems studied here the tip load–displacement envelopes are plotted by joining the peaks of consecutive loops. These plots have better clarity. The rate of stiffness degradation can also be found out from these plots.

Ability of the structure to survive an earthquake depends to a large extent on its ability to dissipate the input energy. Forms of *energy dissipation* include kinetic energy, viscous damping and hysteretic damping, etc. An estimate of the hysteretic damping can be found by the area enclosed in the load–displacement hysteresis loops. It may be noted that a wider loop (i.e. a large difference in ordinates in the ascending and the descending paths) would signify higher hysteretic damping. Cumulative energy dissipated was then calculated by summing up the energy dissipated in consecutive loops through out the test. Failure modes for different specimens are also discussed.

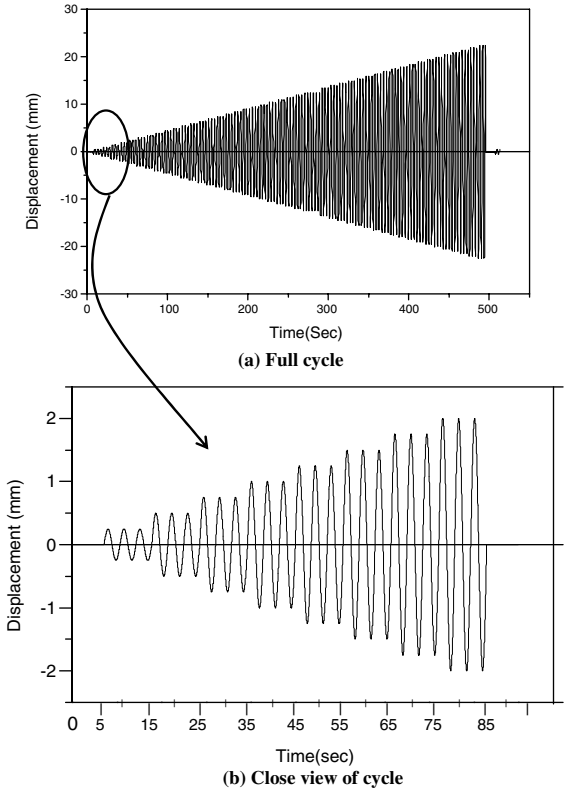

Fig. 8. Predefined displacement cycle applied to beam end.

3.1. Ductile specimens

Beam tip load–displacement graphs for the ductile specimens are plotted in Fig. 9. From the graphs it can be seen that the load at yield was considerably higher in the FRP reinforced specimens than the control specimen. Column 3 of Table 4 summarizes the percentage increase in the yield load. The CP1-D exhibited the highest increase in the yield load followed by the C2L-D, G1L-D and G2L-D specimens. It may be noted that the forces at the tensile face of the beam are shared by the steel and FRP in proportion of their relative stiffnesses. The stiffness of carbon is considerably higher than that of glass. Therefore, for the same tip load, the tensile force in steel is lower in the carbon reinforced specimen than in the glass reinforced specimens. As a result, the steel in the carbon reinforced specimens yields at higher tip loads. The CP1-D specimens are anchored at the joint through a groove. Therefore, they exhibit higher stiffness than other sheet specimens. The specimens with two-layer reinforcement had higher yield loads than the specimens with one layer reinforcements.

Due to FRP reinforcements the displacement at yield increased to a much lesser extent than the load (Column 5, Table 4). Another interesting point is that the glass reinforced specimens had much higher displacement at yield than the carbon reinforced specimens. This is due to the higher stiffness of carbon than that of glass. The ultimate strain in glass is also considerably higher than that in carbon. The CP1 specimens do not follow that trend. The authors believe that better bonding of CP1 specimens through grooves has delayed the onset of yield in them.

The load–displacement envelopes for ductile specimen are plotted in Fig. 10. The envelopes let us compare the relative performance of the specimens. All the FRP reinforced specimens had higher peak loads than the control specimen. The CP1 specimen had the highest peak load followed by the C2L, G2L and G1L specimens. The graph shows the superiority of Type-B arrangement over Type-A reinforcements.

The rate of stiffness degradation is plotted in Fig. 11. All the FRP reinforced specimens had a total loss of stiffness at a higher displacement level than the control specimen. This is a highly desirable phenomenon because the joint collapse can be deferred through FRP reinforcement. The carbon specimens have higher initial stiffness and slower rate of degradation. The CP1 specimens showed some initial gain in stiffness. The authors believe that this is due to the rearrangement in the adhesively bonded groove. The initial stiffness and the ultimate displacements are summarized in Table 5.

The overall performance of the joints can be summarized by the energy dissipation of the structure. The cumulative energy dissipation graphs for the specimens are presented in Fig. 12. The energy dissipation of the FRP reinforced specimens follows closely that of the control specimen. The dissipation of energy is mainly through the yielding if steel. It may be remembered that the FRPs remain elastic until failure. Therefore, not much dissipation of energy is expected through the deformation of the FRP. The only agent of energy dissipation in FRP at this stage is debonding and delamination and the resulting Coulomb damping. However, the FRPs have increased the ultimate deformation of the structure to a large extent. Through higher deformation the FRP reinforced structures have exhibited much higher dissipation of energy. The reasons of higher ultimate deformation in FRP reinforced specimens will be discussed in conjunction with the failure mode. The carbon specimens exhibited higher energy dissipation than the glass specimens.

The photographs of the failed specimens have been presented in Fig. 13. In Fig. 13a the failed control specimen is shown. It may be noted that the beam has failed at the joint through the formation of a hinge. The hinge has formed between the two shear links of the beam. The concrete has spalled in such a fashion that two semicircular surfaces have been created. This has resulted in free rotation of the beam limb with no transfer of bending moment to the column. The reinforcements have been exposed due to spalling of concrete. This has resulted in kinking of the reinforcements. Due to spalling the cracks were too wide and therefore, they did not come in contact in compression. The FRP reinforced

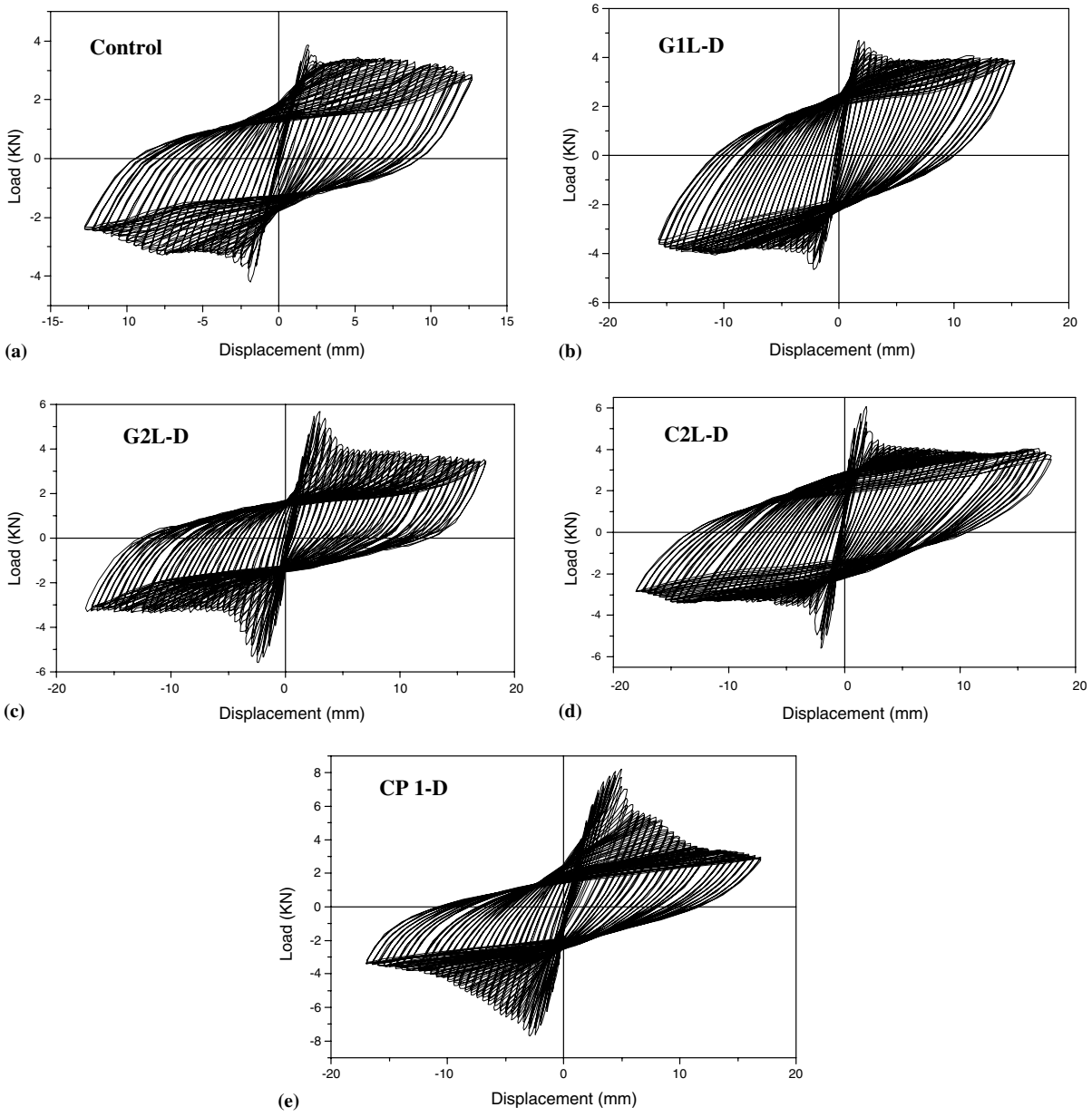

Fig. 9. Load versus deflection for different non-ductile specimens.

Table 4
Yield points of ductile specimens

Specimen	Yield load (N)		Deflection at yield load (mm)	
	Value	% increase	Value	% increase
Control	3.8	–	1.9	–
	−4.15		−1.86	
G1L-D	4.61	21.32	1.71	−10.00
	−4.65	12.05	−2.14	15.05
G2L-D	5.64	48.42	3.02	58.95
	−5.54	33.49	−2.44	31.18
C2L-D	6.0	57.89	1.84	−3.16
	−5.53	33.25	−2.0	7.53
CP1-D	8.215	116.18	4.975	161.84
	−7.67	84.82	−2.87	54.3

specimens, on the other hand, did not have the semicircular failure planes. The failure planes were approximately vertical (Fig. 13b–d). The authors believe that the difference in the failure mode is due to the presence of the FRP wraps. They confined the concrete and did not allow it to spall. As a result, in cyclic opening and closing of cracks the crack surfaces could react against each other in compression. Therefore, the moment resistance of the beam was not lost. This offered higher collapse loads and displacement. To summarize, the main cause of superior performance of the FRP reinforced joints is the continuous confinement provided by the FRP wraps impeded the creation of hinge through the spalling of concrete.

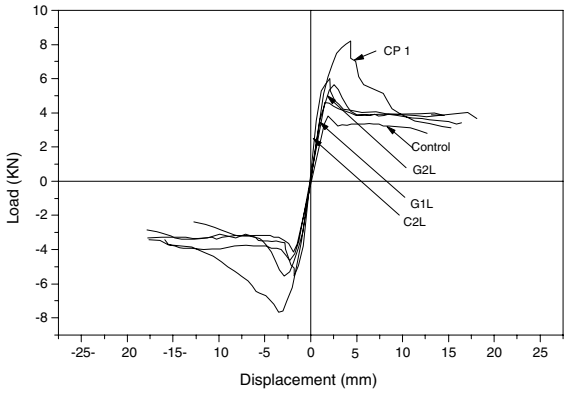

Fig. 10. Load versus deflection envelope plots for ductile specimens.

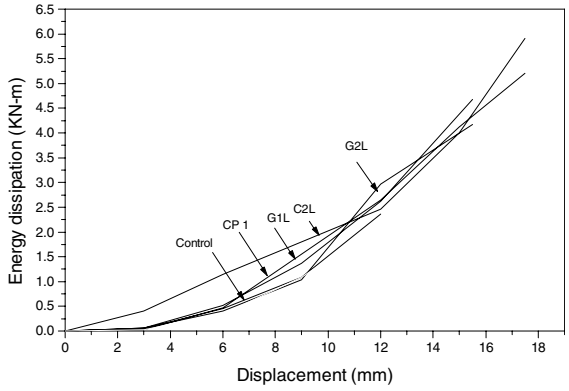

Fig. 12. Energy dissipation versus displacement plots for ductile specimens.

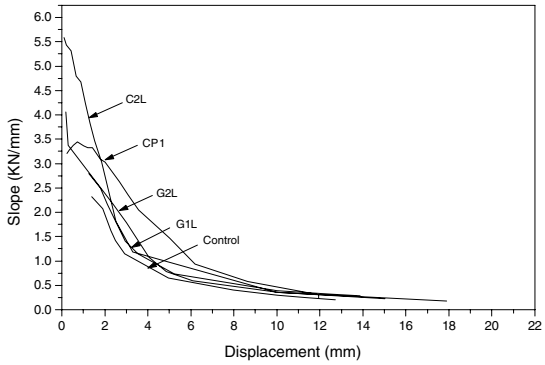

Fig. 11. Stiffness versus deflection plots for ductile specimens.

Fig. 13d shows the failure of CP1 specimens. In this case the CFRP plates were adhesively bonded into the joint by inserting them inside a grove at the joint. The figure shows that the carbon plates have pulled out of the joint and there is no damage to the plate. A thin layer of cement paste is on the surface of the pulled out portion. This shows that the pullout was due to the failure of the cement paste in the groove. The authors expect that this mode will change when larger specimens would be tested; because then the groove could be created through large aggregates. The mechanical anchorage of the large aggregate would help increasing the pull out forces. However, this point needs to be verified through tests. Another difference in these specimens is that the steel reinforcements had torn completely through cup and cone formation. This shows that the deformations in CP1 specimens were large enough to reach the ultimate strain of steel. As a result, the ultimate failure of the joint was not due to the yielding of steel but the pull out of the CFRP plate.

3.2. Rehabbed specimens

A beam tip load–displacement relationship for undamaged ductile specimen and rehabbed specimen is plotted in Fig. 14. Also the load versus displacement envelops for the same specimens are plotted in Fig. 15. It shows that the use of composite system did not only restore the original capacity of damaged specimen, but also upgraded the ultimate load capacity by 55%. Also displacement at ultimate load increased by 30%. Stiffness versus displacement curves (Fig. 16) show that there is 48% increase in initial stiffness. An increment of 57% is observed in energy dissipation capacity of

Table 5
Ultimate points in ductile specimens

Specimen	Initial stiffness		Ultimate deflection		Energy dissipation capacity (KNm)	
	Value (KN/mm)	% increase	Value (mm)	% increase	Value	% increase
Control	2.32	–	12.7 −12.73	–	2.37	–
G1L-D	2.80	17.14	14.56 −15.86	14.65 24.59	4.68	97.47
G2L-D	4.06	75.00	16.41 −17.78	29.21 39.67	4.18	76.37
C2L-D	5.59	140.94	18.14 −17.86	42.83 40.30	5.96	151.48
CP1-D	3.28	41.37	15.32 −17.61	20.63 38.42	5.21	119.83

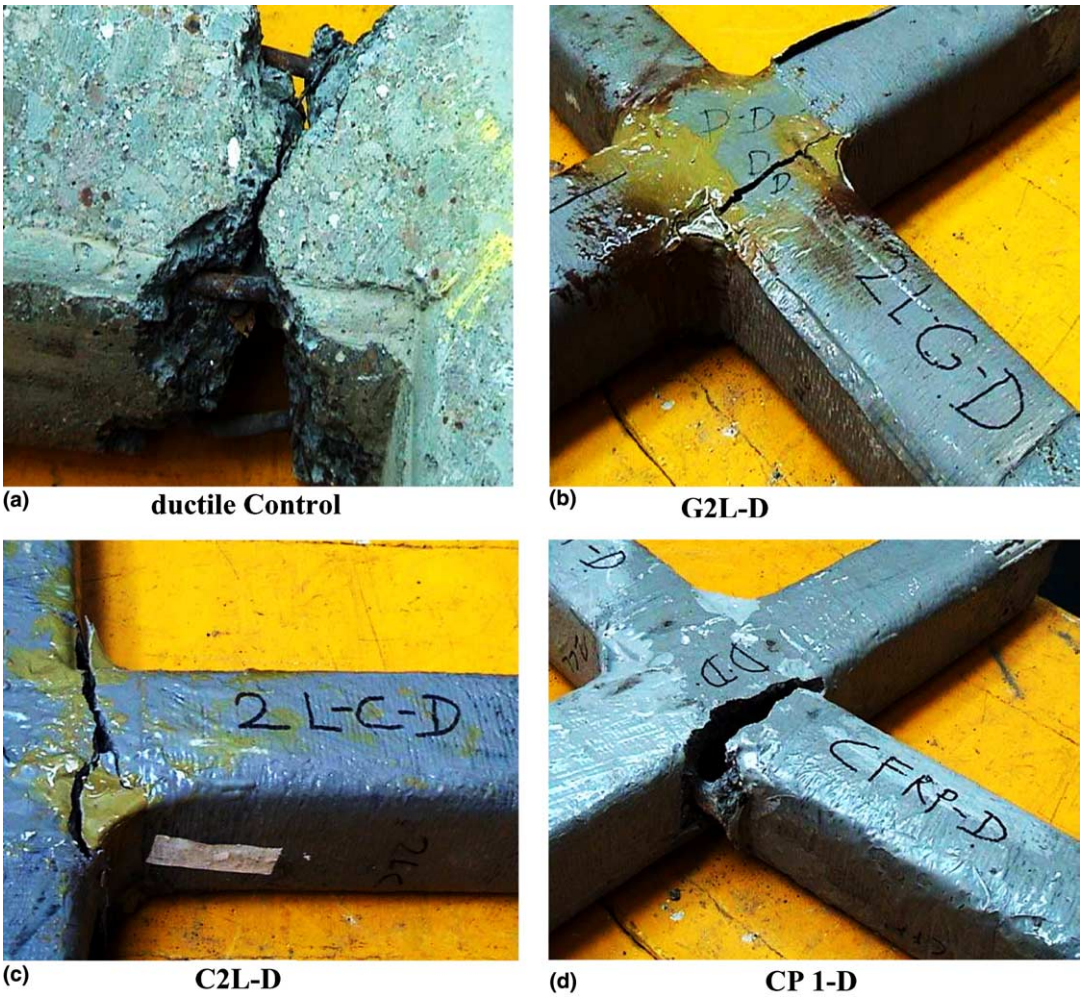

Fig. 13. Failure patterns for ductile specimens.

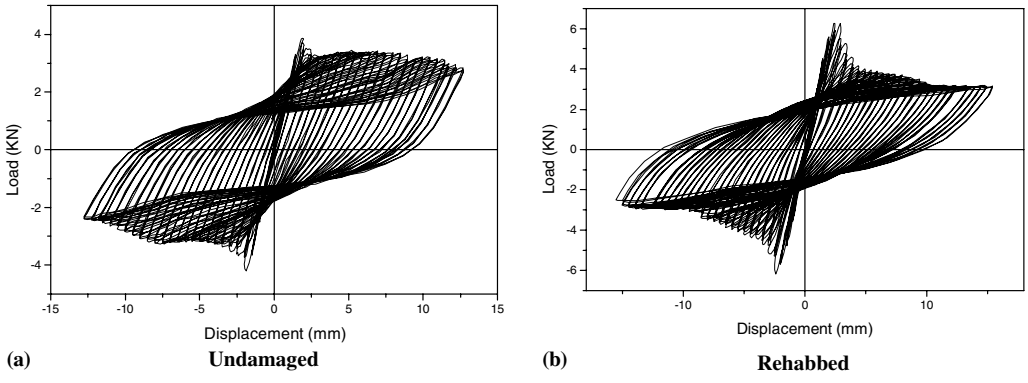

Fig. 14. Load versus deflection for undamaged and rehabbed specimens.

structure after the rehabilitation (Fig. 17). The detailed results of rehabbed specimen are given in Tables 6 and 7.

3.3. Non-ductile specimens

Beam tip load–displacement graphs for the non-ductile specimens are plotted in Fig. 18. From the graphs it can be seen that the load at yield was considerably higher in the FRP reinforced specimens than the control specimen. Column 3 of Table 8 summarizes the percentage increase in the yield load. The G2L-ND exhibited the highest increase in the yield load followed by the C2L-ND, CP1-ND and C1L-ND specimens. The specimens with two-layer reinforcement had higher

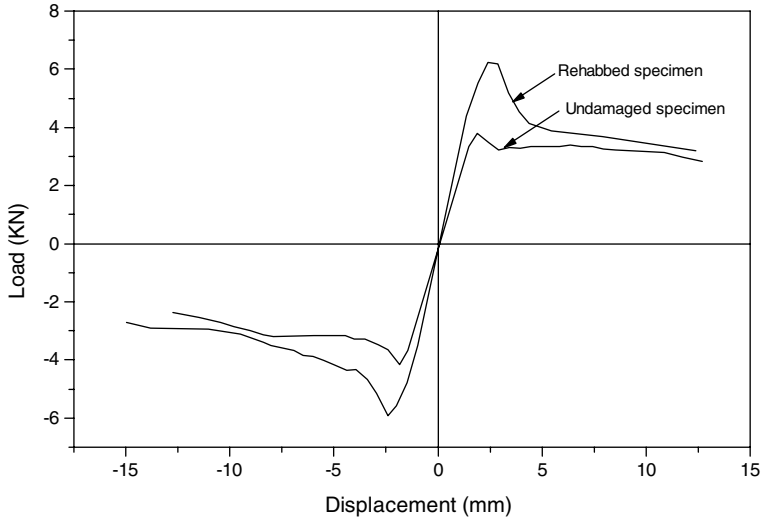

Fig. 15. Load versus deflection envelope plots for rehabbed and undamaged specimen.

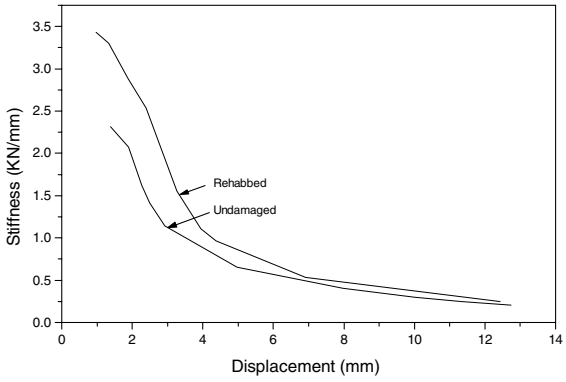

Fig. 16. Stiffness versus deflection plots for undamaged and rehabbed Specimens.

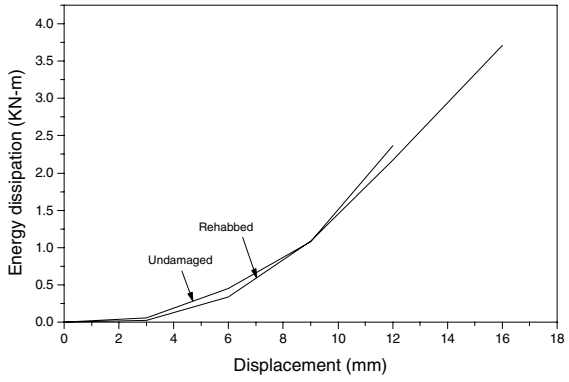

Fig. 17. Energy dissipation versus deflection plots for undamaged and rehabbed specimens.

Table 6
Yield points of undamaged and rehabilitated specimens

Strengthening configuration	Yield load		Deflection at yield load	
	Value (N)	% increase	Value (mm)	% increase
Undamaged	3.8	–	1.9	–
	−4.15		−1.86	
Rehabbed	6.31	66.05	2.46	29.47
	−5.97	43.86	−2.42	30.11

Table 7
Ultimate points in undamaged and rehabilitated specimens

Specimen	Initial stiffness		Ultimate deflection		Energy dissipation capacity (KNm)	
	Value (KN/mm)	% increase	Value (mm)	% increase	Value	% increase
Control	2.32	–	12.7	–	2.37	–
			−12.73			
Rehabbed	3.43	47.84	12.38	−2.52	3.71	56.54
			−14.97	17.6		

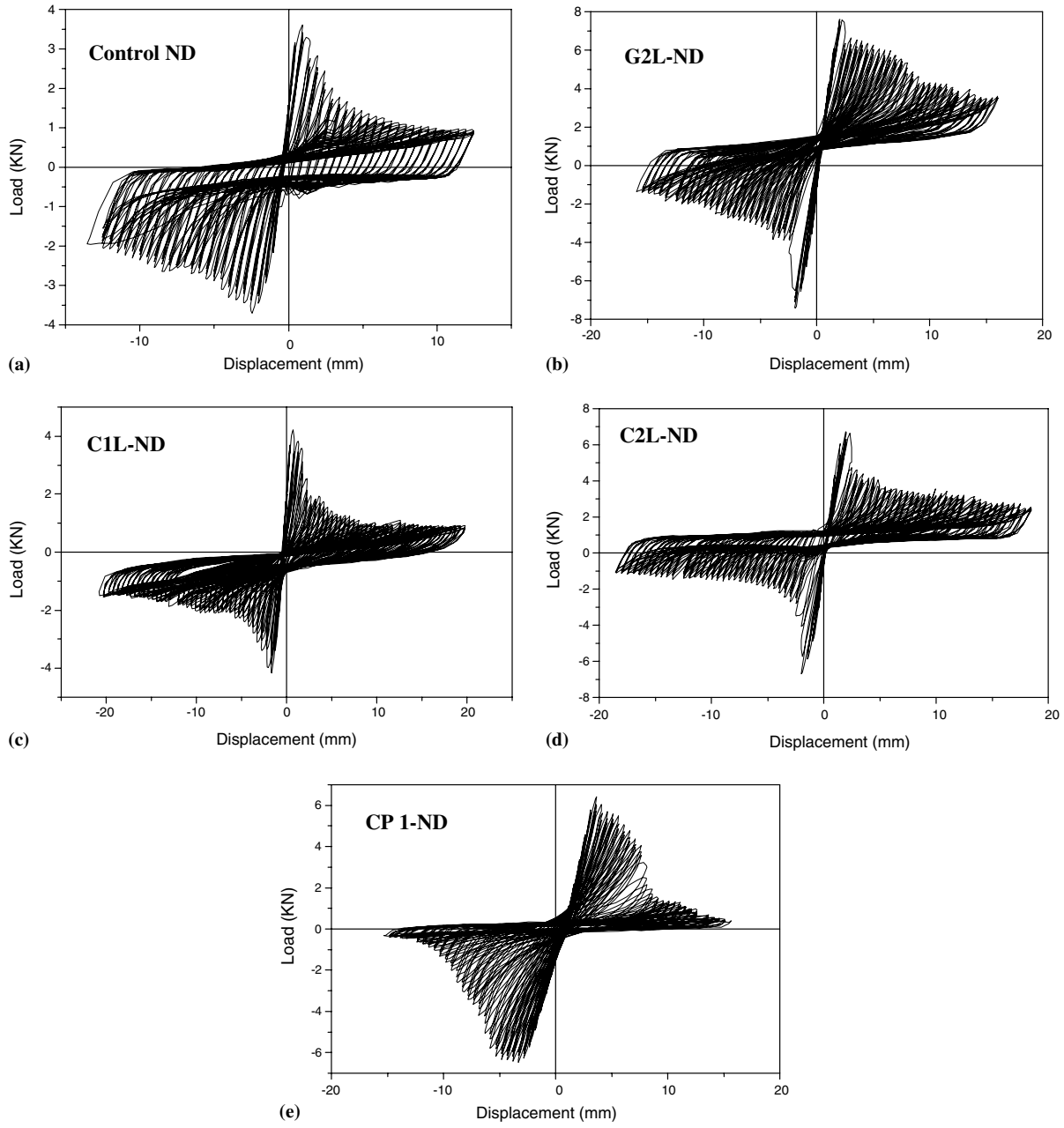

Fig. 18. Load versus deflection for different non-ductile specimens.

yield loads than the specimens with one layer reinforcements.

Due to FRP reinforcements the displacement at yield increased to a much lesser extent than the load (Column 5, Table 8). Similar to the previous ductile specimens the glass reinforced specimens had a much higher displacement at yield than the carbon reinforced specimens. The CP1-ND specimens do not follow that trend. The authors believe that better bonding of CP1-ND specimens through grooves has delayed the onset of yield in them.

The load–displacement envelopes for the ductile specimens are plotted in Fig. 19. The envelopes let us compare the relative performance of the specimens. All the FRP reinforced specimens had larger areas under the envelopes than the control specimen. The G2L-ND specimen had the largest envelope area followed by the C2L-ND, CP1-ND and C1L-ND specimens. The graph shows superiority of glass reinforcements over carbon reinforcement in case of non-ductile specimen.

The rate of stiffness degradation is plotted in Fig. 20. All the FRP reinforced specimens had a total loss of stiffness at a higher displacement level than the control specimen. This is a highly desirable phenomenon because the joint collapse can be deferred through FRP reinforcement. The glass specimens have higher initial

Table 8
Test results for non-ductile specimens

Specimens	Yield load		Deflection at yield load	
	Value (N)	% increase	Value (mm)	% increase
Control-ND	3.73	–	1.64	–
	−3.6		−1.70	
G2L-ND	7.6	103.75	1.829	15.24
	−7.43	106.38	2.195	29.11
C1L-ND	4.2	12.60	1.34	−18.29
	−4.14	10.99	−1.46	−14.11
C2L-ND	6.69	79.36	1.71	4.27
	−6.67	85.28	−2.1	23.53
CP1-ND	6.28	68.36	2.92	78.05
	−6.39	77.5	−4.02	136.47

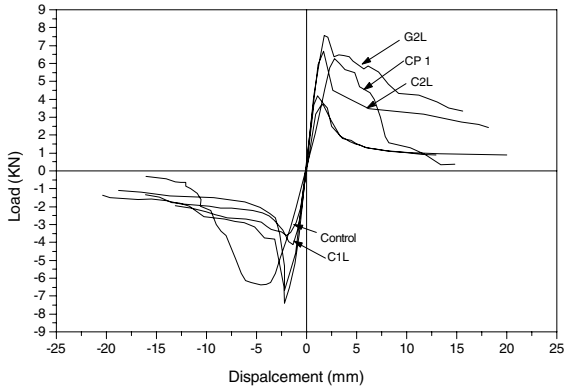

Fig. 19. Load versus deflection envelope plots for non-ductile specimens.

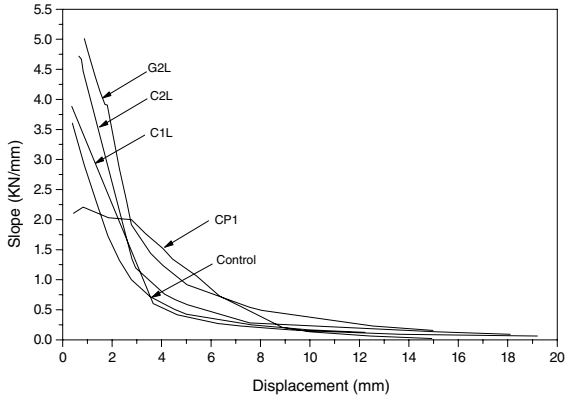

Fig. 20. Stiffness versus deflection plots for non-ductile specimens.

stiffness and slower rate of degradation. The CP1 specimens showed highest stiffness between displacement levels of 3–6 mm. The authors believe that this is due to the rearrangement in the adhesively bonded groove. The initial stiffness and the ultimate displacements are summarized in Table 9.

The overall performance of the joints can be summarized by the energy dissipation of the structure. The cumulative energy dissipation graphs for the specimens are presented in Fig. 21. The energy dissipation of the FRP reinforced specimens follows closely that of the control specimen. The dissipation of energy is mainly through the yielding if steel. In absence of adequate development length considerable loss in energy dissipation capacity of control specimen is observed. FRPs have increased the ultimate deformation of the structure

Table 9
Ultimate points in non-ductile specimens

Specimen	Initial stiffness		Ultimate deflection		Energy dissipation capacity (KN m)	
	Value (KN/mm)	% increase	Value (mm)	% increase	Value	% increase
Control-ND	3.57	–	12.81	–	0.695	–
			−13.11			
G2L-ND	5.05	41.46	15.43	20.45	2.196	215.97
			−16.04	22.35		
C1L-ND	3.91	9.52	19.87	55.11	1.42	104.32
			−20.30	55.07		
C2L-ND	4.73	32.49	18.11	41.37	1.47	111.51
			−18.72	42.79		
CP1-ND	2.1	−41.17	14.87	16.08	1.116	60.57
			−15.01	14.49		

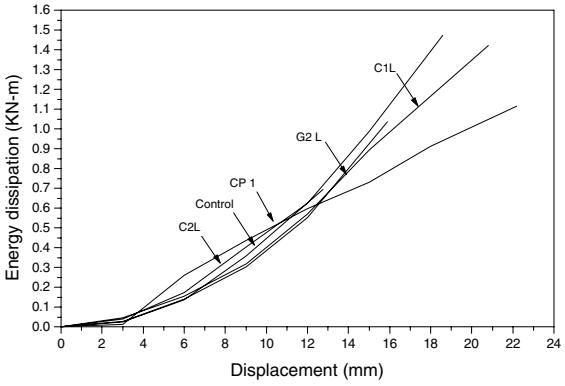

Fig. 21. Energy dissipation versus displacement plots for non-ductile specimens.

to a large extent. Through higher deformation the FRP reinforced structures have exhibited much higher dissipation of energy. The reasons of higher ultimate deformation in FRP reinforced specimens will be discussed in conjunction with the failure mode. The glass reinforced specimens exhibited higher energy dissipation than the carbon-reinforced specimens. The relative increase in energy dissipation capacity is more in case of non-ductile specimen over the ductile specimen, due to lower energy dissipation capacity of control specimen.

The photographs of the failed specimens have been presented in Fig. 22. In Fig. 22a the failed control specimen is shown. It may be noted that the beam has failed

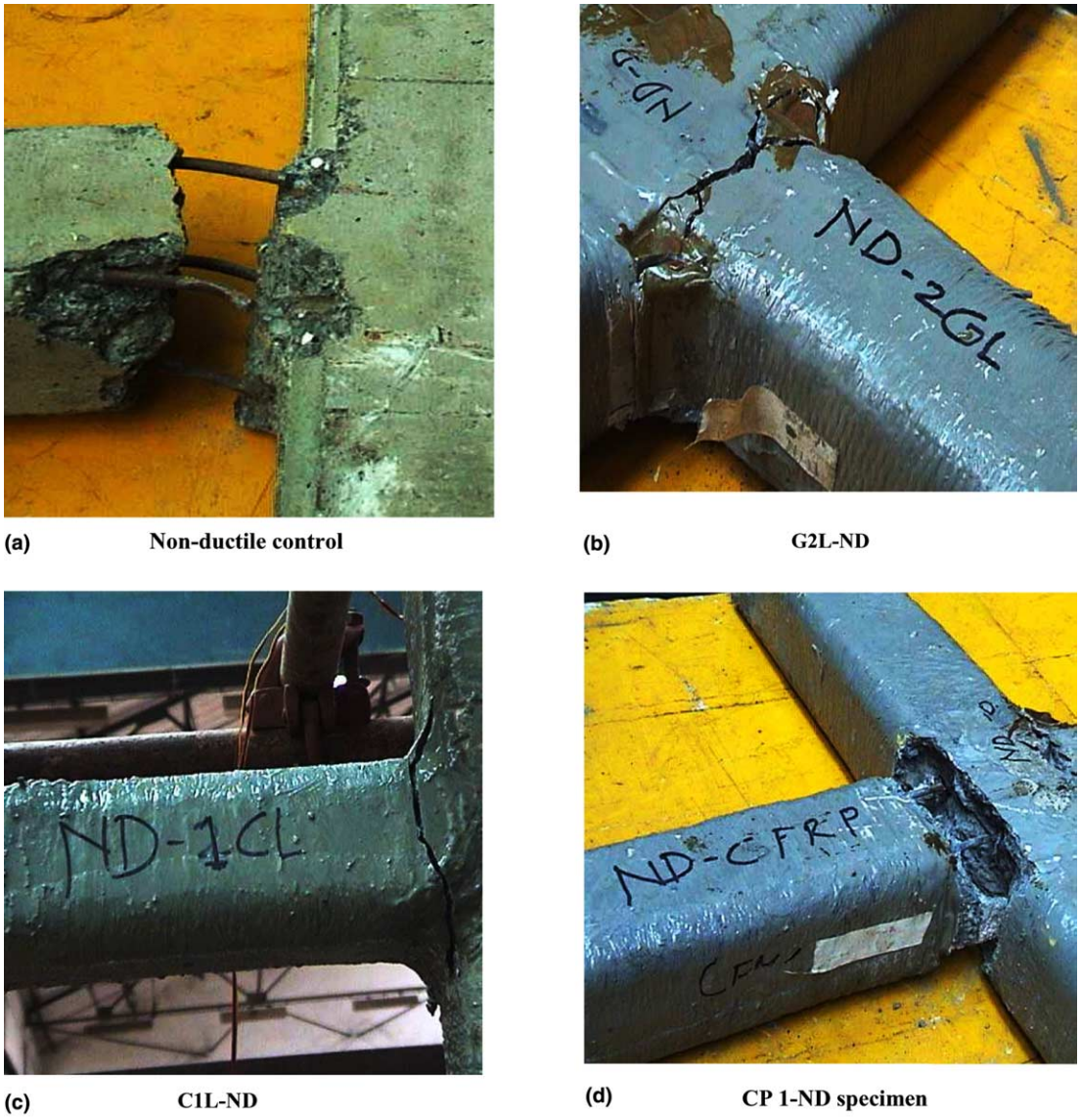

Fig. 22. Failure patterns for non-ductile specimens.

at the joint by pull out of steel reinforcement. Lack of development length prevented the formation of plastic hinge. The FRP reinforced specimens, on the other hand, did not have the reinforcement pull out. The failure planes were approximately vertical (Fig. 22b–d). The authors believe that the difference in the failure mode is due to the presence of the FRP overlays and wraps. They confined the concrete and did not allow it to spall. FRP Overlays helped to hold the beam in its position. As a result, the cracked concrete surfaces closed and they could react against each other at subsequent cycles. Therefore, the moment resistance of the beam was not lost. This offered higher collapse loads and displacement. To summarize, the main cause of superior performance of the FRP reinforced joints is the continuous confinement provided by the FRP wraps and overlays impeded the pull out of reinforcement through the inadequately detailed specimens.

Fig. 22d shows the failure of CP1-ND specimens. The failure pattern is similar to its counterpart ductile specimen discussed previously. The figure shows that both the CFRP plates and steel reinforcement have pulled out of the joint and there is no damage to the plate. A thin layer of cement paste is on the surface of the pulled out portion. This shows that the pullout was due to the failure of the cement paste in the groove. As a result, the ultimate failure of the joint was due to the pull out of both the steel bars and the CFRP plate.

4. Conclusions

Both glass and carbon composite materials can be efficiently used for seismic retrofitting as well as rehabilitation of reinforced concrete joints. Joints exhibit enhanced strength regardless of reinforcement detailing and damage state. Considerable increase in yield load can be achieved by use of these materials. Yield load and initial stiffness depends on numbers of overlays provided in the joint area. Specimens strengthened using CFRPs show stiffer behavior than GFRP strengthened specimens. Energy dissipation capacity can be increased with the use of small amount of composites. Test on rehabbed specimen suggests that FRP not only restores its original strength but there is considerable enhancement in its yield load, initial stiffness and energy dissipation capacity.

Acknowledgment

The authors would like to acknowledge the donation of fiber and adhesive materials from Sika AG. The financial support received from Board of Nuclear research, India is thankfully acknowledged.

References

[1] Alcocer S, Jisra JO. Strengthening of reinforced concrete frame connection rehabilitated by jacketing. ACI Struct J 1993;90(3):249–61.
[2] Tsonos AG. Lateral load response of strengthened reinforced concrete beam to column joint. ACI Struct J 1999;96(1):46–56.
[3] Beres A, EI-Borgi S, White RN, Gergely P. Experimental results of repaired and retrofitted beam-column joint tests in lightly reinforced concrete frame building. Technical report NCEER-92-0025, State University New York at Buffalo, 1992.
[4] Ghobarah A, Aziz TS, Biddah A. Rehabilitation reinforced concrete frame connections using corrugated steel jacketing. ACI Struct J 1997;4(3):283–94.
[5] Pantelides CP, Gergely I, Reaveley LD, Nuismer RJ. Rehabilitation of cap beam-column joints with carbon fiber jackets. Proc 3rd Int Symp on non-metallic (FRP) reinforcement for concrete structures, Sapparo Japan, vol. 1. Tokyo: Japan Concrete Institute; 1997. p. 587–95.
[6] Pantelides CP, Gergely J, Reaveley LD, Volnyy VA. Retrofit of PC bridge pier with CFRP advance composites. J Struct Eng ASCE 1999;125(10):1094–9.
[7] Li J, Bakoss SL, Samali B, Ye L. Reinforcement of concrete beam-column connections with hybrid FRP sheet. Compos Struct 2000;47:805–12.
[8] Granata JP, Parvin A. An experimental study on Kevlar strengthening of beam column connection. Compos Struct 2001;53:163–71.
[9] Castellani A, Negro P, Colombo A, Grandi A, Ghisalberti G, Castellani M. Carbon fiber reinforced polymers (CFRP) for strengthening and repairing under seismic actions. Special Publication No. I.99.41, European Laboratory for Structural Assessment, Joint Research Center, Ispra, Italy, 1999.
[10] Geng ZJ, Chajes MJ, Chou TW, Pan DYC. The retrofitting of reinforced concrete column-to-beam connections. Compos Sci Technol 1998;58:1297–305.
[11] Mosallam A. Seismic repair and upgrade of structural capacity of reinforced concrete connections: Another opportunity for polymer composites. In: Proc Int Composites Expo. Cincinnati: 1999. p. 1–8.
[12] Gergely I, Pantelides CP, Nuismer RJ, Reaveley LD. Bridge pier retrofit using fiber reinforced plastic composite. J Compos Construct, ASCE 1998;2(4):165–74.
[13] Gergely J, Pantelides CP, Reaveley LD. Shear strengthening of RCT-joints using CFRP composites. J Compos Construct, ASCE 2000;4(2):56–64.
[14] Ghobarah A, Said A. Shear strengthening of beam-column Joints. Eng Struct 2001;24:881–8.
[15] Prota A, Nani A, Manfredi G, Cosenza E. Seismic upgrade of beam-column joints with FRP reinforcement . Industria Italiana del Cemento, November 2000. p. 1–17.
[16] Antonopoulos CP, Triantafillou TC. Experimental investigation of FRP-strengthened RC beam-column joints. J Compos Construct 2003;7(1):39–49.
[17] Mosallam SA. Strength and ductility of reinforced concrete moment frame connections strengthened with quasi-isotropic laminates. Composites: Part B 2000;31:481–97.
[18] El-Amoury T, Ghobarah A. Seismic rehabilitation of beam-column joint using GFRP sheets. Eng Struct 2002;24:1397–407.

[19] D'Ayala D, Penford A, Valentini S. Use of FRP fabric for strengthening of Reinforced concrete beam-column joints. In: 10th Int. conference on structural faults and repair. London: July 2003.
[20] Antonopoulos CP, Triantafillou TC. Analysis of FRP-strengthened RC beam-column joints. J Compos Construct 2002;6(1): 41–50.
[21] Granata JP, Parvin A. Investigation on the effects of fiber composites at concrete joints. Composites: Part B 2000;31: 499–509.
[22] Gergely J, Pantelides CP, Reaveley LD. Shear strengthening of RCT-joints using CFRP composites. J Compos Construct ASCE 2000;4(2):56–64.
[23] Mukerjee A, Kalyani AR. Upgradation design of reinforced concrete frames with fiber reinforced composites. J Compos Construct ASCE, submitted for publication.